



# Beamforming array optimisation and phase averaged sound source mapping on a model wind turbine

Zebb PRIME<sup>1</sup>; Con DOOLAN; Branko ZAJAMSEK

The University of Adelaide, Australia

## ABSTRACT

Beamforming is an array processing technique often used to localise sound sources. This paper details the design and testing of a new planar microphone array in the School of Mechanical Engineering at the University of Adelaide which will be used for localising the noise generation from a model wind turbine. The array microphone locations were found using a constrained bi-objective optimisation to find a good compromise between the array resolution, also known as beamwidth, and the maximum value of spurious lobes, known as the maximum side-lobe level. Aggregate and phase averaged beamforming results of a rotor rig experiment are presented.

Keywords: Beamforming, Sparse Array, Aeroacoustics

I-INCE Classification of Subjects Number(s): 14.5.4 74.6 74.7

## 1. INTRODUCTION

Beamforming is an array signal processing technique which is used to either enhance the signal from a chosen source, or to produce a map of sound sources (source localisation). In the context of acoustics, beamforming and beamforming arrays are often known by terms 'phased array', 'acoustic telescope', 'antenna' or 'acoustic camera'.

The array configuration has a direct influence on the achievable spatial resolution when beamforming. Line arrays achieve good resolution along an axis parallel to the array, but poor resolution along other axes. Similarly, good planar resolution can be achieved using a planar array of microphones, however for a regular spatial array the number of microphones required to prevent spatial aliasing at even moderate frequencies while maintaining an acceptable resolution is prohibitive. Instead, an appropriately designed sparse array can achieve good resolution and prevent spatial aliasing; the downside being the emergence of 'side-lobes' around the source location.

When beamforming on an acoustic source far enough away that the incoming pressure waves can be assumed to be planar, also known as far-field beamforming (not to be confused with the acoustic far-field), the array response function simplifies such that global optimisation can be performed on the array response, for example the B&K array (1, 2) has been optimised to minimise side-lobes subject to microphones being located on a spoke. However when beamforming on a source close enough that the pressure waves must be assumed to be spherical, also known as near-field beamforming (again, not to be confused with the acoustic near-field), no global expression for the response exists. Several authors have developed guidelines for constructing near-field sparse arrays to achieve adequate resolution and side-lobe levels (measured using the Maximum Side-lobe Level (MSL) in a given scan plane) based on spirals (3, 4, 5), as the inter-microphone spacings of a spiral are guaranteed to be unique. A comparison of several of these popular designs was performed by Prime and Doolan (6), where it was shown that multi-spiral and multi-spoke designs achieved the best resolution with acceptable MSLs.

In this paper we document the design, construction and testing of a new beamforming array at the School of Mechanical Engineering, The University of Adelaide, and present some results of beamforming on an unloaded rotor rig, including aggregate and phase-averaged results. This paper is structured as follows: firstly the microphone placement via bi-objective optimisation is presented in Section §2.1; followed by details of its construction in Section §2.2. The results of beamforming on the rotor rig are presented in Section §3; and conclusions drawn in Section §4.

---

<sup>1</sup>zebb.prime@adelaide.edu.au

## 2. SCHOOL OF MECHANICAL ENGINEERING BEAMFORMING ARRAY

A new beamforming array was commissioned for the testing of noise generation from a rotor rig in a wind tunnel, however it is expected to have a wider range of applications, such as environmental sound source localisation.

The array uses 64 GRAS 40PH phase matched microphones located on a planar array in order in order to do wide-band beamforming. Each microphone was connected to a channel in a PXIe-4499 24bit simultaneous sample and hold data acquisition card.

This section details how the microphone locations were chosen, the array construction, calibration, and compares experimental and theoretical performance of the array.

### 2.1 Array optimisation

The response of an array at a frequency  $f$  and (scan) location  $\vec{x}_p$  to a point source located at  $\vec{x}_s$  and normalised to the source location is given by (5):

$$Y(f, \vec{x}_p, \vec{x}_s) = \left( \sum_{n=1}^N \frac{r_s}{r_n} \right)^{-1} \sum_{n=1}^N \frac{r_s}{r_n} \exp \left\{ 2\pi f j \left[ \frac{(r_s - r_p) - (r_n - r'_n)}{c} \right] \right\}, \quad (1)$$

where  $N$  is the number of microphones;  $r_s$  is the distance from the source to the origin of the array;  $r_p$  is the distance from the origin to the focus point;  $r_n$  is the distance from the source to the  $n$ -th microphone;  $r'_n$  is the distance from the  $n$ -th microphone to the focus point; and  $c$  is the speed of sound. An example array response is shown in Figure 1. The array resolution, also known as the beamwidth, can be evaluated as the width at a

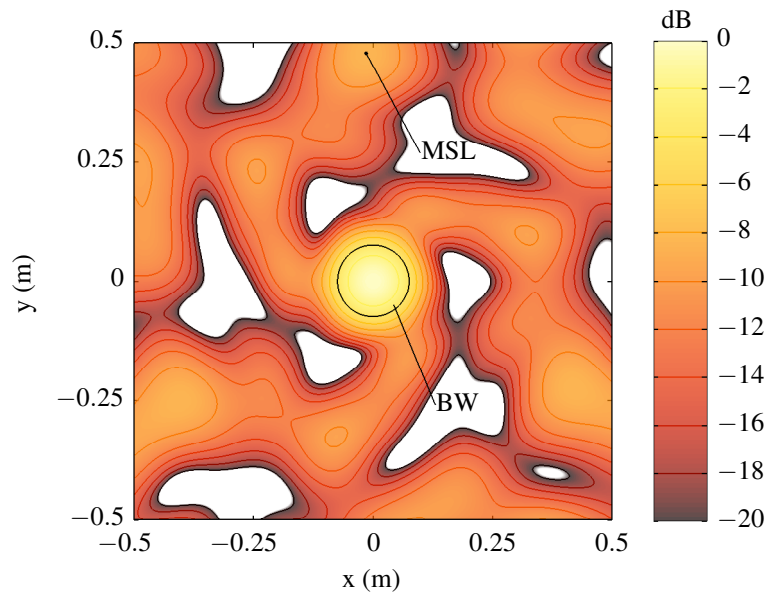


Figure 1 – Example array response, with beamwidth and MSL highlighted.

point 3 dB down from the source location, and the MSL is the maximum point outside of the main lobe, as shown in Figure 1.

Due to the three-dimensional dependence on the distance from microphones to scan locations, the  $r$  terms in Equation (1), generalising the array response is difficult. If all of the geometric terms are scaled by a factor, say  $p$ , and the frequency is reduced by the factor  $1/p$ , then we will have the same response as the original system, therefore the array response can be somewhat generalised using a suitable geometric factor. In this case, an appropriate choice is the array aperture—a linear measure of the array sensing area—which for a circular array is just the diameter.

The beamwidth is known to scale linearly with wavelength,  $\lambda$ , and from the discussion above scales with the inverse of array aperture,  $D$ , thus an expression for the beamwidth,  $BW$  is:

$$BW = \frac{k\lambda}{D}, \quad (2)$$

where  $k$  is a beamwidth constant for a given array geometry.

Similarly, the MSLs can be somewhat generalised by evaluation at a range of normalised diameters per wavelength,  $\frac{D}{\lambda}$ . For optimisation, these MSL levels need to be reduced to a scalar cost value. This was achieved by summing the difference between the evaluated MSLs and the 80% level of MSL expectation for a random array from Steinberg (7), which is given by:

$$\text{PMSL}_{0.8} = \frac{B + 1 + 2/B}{N}, \quad (3)$$

$$B = -\ln(1 - 0.8^{\frac{1}{n}}), \text{ and} \quad (4)$$

$$n = \frac{D}{\lambda} (1 + \sin \theta), \quad (5)$$

where  $N$  is the number of microphones, and  $\theta$  is angle between the centre of the array and the source.

Various popular sparse array designs from aeroacoustics, as well as a less constrained pattern consisting of multiple circles of microphones, were input into the NOMAD nonlinear mesh-adaptive direct search black box biobjective optimisation program (8, 9). Each array consisted of 64 microphones, and the MSL cost and beamwidth constant were evaluated on an circular plane parallel to the array with a radius of  $D$ , at a location  $z/D = 1$  away from the array. The beamwidth constant was evaluated at a frequency equivalent to a wavelength of  $\frac{D}{8}$ , and the MSLs were evaluated at the frequencies:

$$f_{MSL} = 2^{n/3} \frac{D}{8}, \quad n = 0 \dots 12, \quad (6)$$

i.e. equal to 1/3 octave band spacings starting from  $\frac{D}{8}$ .

The array types and varied parameters evaluated using the optimisation procedure are shown in Table 1.

Table 1 – Array types and input parameters evaluated during the optimisation process.

Array type	Optimisation parameters
1. Underbrink (4), 7 arms, 9 mics/arm +1 at origin	$r_0$ (minimum radius), $v$ (spiral angle)
2. Underbrink (4), 9 arms, 7 mics/arm +1 at origin	$r_0$ (minimum radius), $v$ (spiral angle)
3. B&K (2), 7 arms, 9 mics/arm +1 at origin	$r_0$ (minimum radius), $\phi$ (spoke angle) $d_n$ (normalised mic position on spoke)
4. B&K (2), 9 arms, 7 mics/arm +1 at origin	$r_0$ (minimum radius), $\phi$ (spoke angle) $d_n$ (normalised mic position on spoke)
5. Circles, 7 mics/circle, 9 circles +1 at origin	$r_n$ (radius of each circle), $\phi_n$ (circle offset angle)
6. Circles, 9 mics/circle, 7 circles +1 at origin	$r_n$ (radius of each circle), $\phi_n$ (circle offset angle)

The results of the optimisation are shown in Figure 2 as a Pareto front, which is the optimal values of each parameter as they trade-off with the other parameter. The results show that for this scenario, an array consisting of 7 concentric circles, with each circle containing 9 microphones has a smaller MSLs for a given beamwidth constant, and hence with a slight trade-off towards reduced MSLs—the black point in Figure 2—was used as the design of the new beamforming array. The results also show that the Underbrink arrays have a small Pareto front, but with good performance, suggesting this design performs well, and the performance is less sensitive to design parameters than the other designs considered.

The microphone locations of the chosen design point are shown in Figure 3.

## 2.2 Array construction

The array was designed to investigate aeroacoustic sound sources, including the rotor-rig mentioned in Section §3, which have signals of interest at low frequencies. The array was therefore designed to have the smallest beamwidth possible, which requires the largest aperture possible. The material used for the array construction was 12 mm Aluminium plate, which was water-jet cut to minimise the error in microphone locations, which directly influence the quality of the beamforming results. The largest array aperture that was practical for the Aluminium plate stock and water-jet cutting size was 1.5 m, hence the array was designed to this size.

To reduce weight, large areas without microphones were cut away during the water-jet cutting process.

The microphones are held using cable glands to accurately and positively hold them in place.

A frame to hold the array was constructed from MayTec extruded Aluminium, designed to allow the frame to slide up and down, as well as pitch forward and backward.

A photograph of the final assembled array is shown in Figure 4

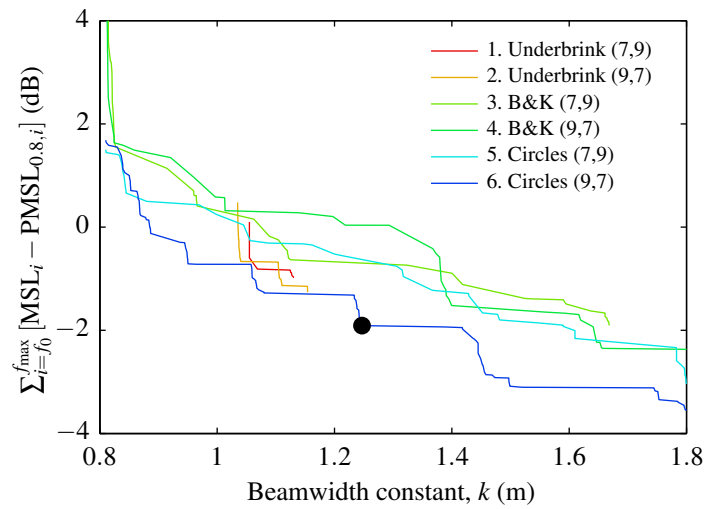


Figure 2 – Pareto front results of the biobjective optimisation applied to different array designs. The black dot indicates the chosen design point.

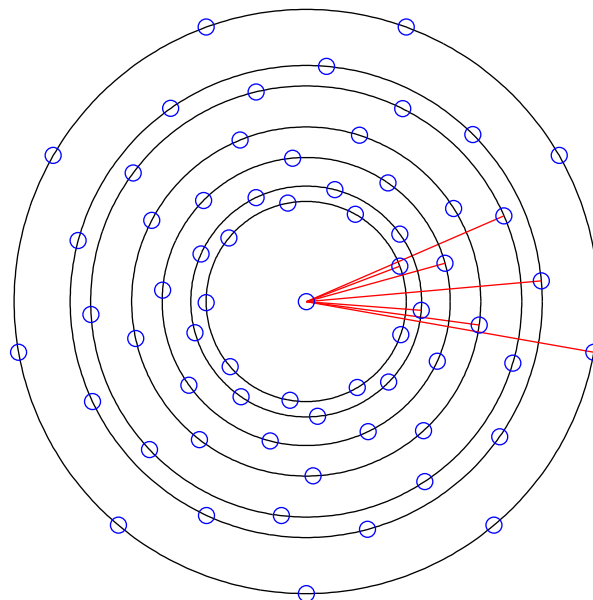


Figure 3 – Microphone locations of the chosen optimised design point, based on the concentric circle design, with 7 circles of 9 microphones each. The blue circles represent microphone locations, and the red lines indicate the offset of each ring of circles from horizontal.



Figure 4 – The assembled School of Mechanical Engineering beamforming array.

### 3. ROTOR RIG

As part of an ongoing project into rotor noise generation, a rotor rig has been constructed. The rotor rig consists of three NACA0012 blades, driven by a 1 kW motor/generator, and instrumented with an encoder, torque sensor, and slip-rings to allow in-hub and on-blade instrumentation.

In a series of tests, the rotor rig was placed in the Anechoic room in The School of Mechanical Engineering, The University of Adelaide, with the beamforming array placed directly in front of the rotor at a distance of approximately  $z = 1.5$  m. The rotor was driven to a speed of 900 rpm with unloaded blades ( $\alpha = 0^\circ$ ), and the acoustic signal and position (encoder signal) logged for  $T = 60$  s at a sample rate of  $f_s = 2^{16}$  Hz.

A photograph of the rotor rig in the Anechoic room with the array placed in front of it is shown in Figure 5.

#### 3.1 Aggregate beamforming results

Results of beamforming on the rotor without any attempt to de-rotate the source are shown in Figure 6. Data was used from 1 s after the rotor reached the run speed until the end of the record, and standard cross-spectra beamforming (5) was applied. The cross-spectrum matrix was calculated using Welch's method with a Hanning window, Fast Fourier Transform (FFT) size of  $2^{13}$  samples, with an overlap of  $2^{12}$  samples, resulting in 772 blocks used for a spectral estimate with a 95% confidence interval of  $[-0.32 \quad 0.31]$  dB. During this period, the rotor completed 725 revolutions, thus the resulting sound maps will be a good estimate of the average rotor sound generation.

The results in Figure 6 at higher frequencies show the sound is predominately generated around the tip of the blades, where the relative velocity is the highest. At lower frequencies, the resolution of the array is so large that the precise source location is difficult to determine. Future work will look at the application of advanced techniques—such as deconvolution—to improve the resolution and dynamic range of these results.

#### 3.2 Phase-averaged beamforming results

While the results in Section §3.1 show the average sound generation from the rotor rig, it can be useful to de-rotate the results and show the sound generation at a particular rotor angle. In this work, the rotor noise generation is de-rotated by averaging the sound generation at a particular rotor angle (phase-averaged).

The standard cross-spectral beamforming algorithm calculates a cross-spectral matrix estimate using Welch's method over the entire time record, and as such is not suitable for phase-averaged results. Instead,

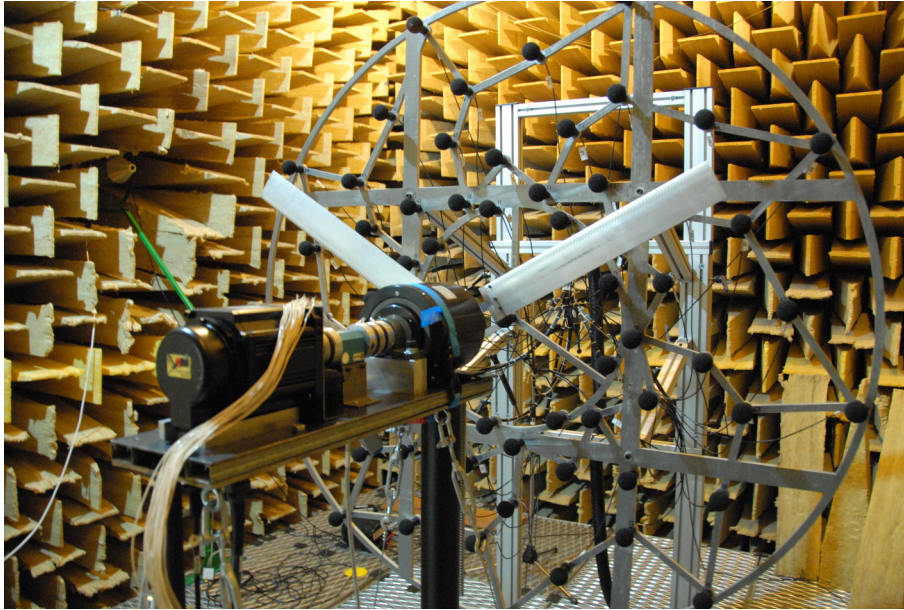


Figure 5 – Rotor rig and beamforming array in the Anechoic room at The University of Adelaide. Note that during the experiment the array was located further away from the array than pictured here.

small pieces of data around the desired rotor angle can be taken, and used to calculate the sound contributions.

For each time the rotor passes through the desired de-rotated angle,  $\theta_0$ , the pressure record is delayed and summed according to the propagation delay between each grid point to each microphone:

$$\bar{p}_k(t_i) = \frac{1}{\sqrt{N \sum_{n=1}^N (r_{1,k}/r_{n,k})^2}} \sum_{n=1}^N \frac{r_{1,k}}{r_{n,k}} p_n \left( t_i - \frac{r_{n,k}}{c} \right), \quad (7)$$

$$t_i = t(\theta(t) = \theta_0) + [-\Delta t_\theta, \Delta t_\theta], \quad (8)$$

where  $\bar{p}_k(t_i)$  is the delayed and summed pressure at grid location  $k$  corresponding to a time record of width  $2\Delta t_\theta$  about the  $i$ -th time that  $\theta(t) = \theta_0$ ,  $r_{n,k}$  is the distance between microphone  $n$  and the scan grid location  $k$ , and  $p_n(t)$  is the pressure record of microphone  $n$ . The terms out the front of the summation and the pressure record correspond to amplitude corrections for each signal, and is equivalent to the amplitude corrections in the steering vectors for cross-spectral beamforming, in this case a Formulation 4 steering vector from Sarradj (10).

Each delayed and summed pressure record is then used in Welch's method to estimate the power spectrum at that grid location:

$$P_k(f) = \frac{2}{IF_s \sum_{l=1}^L w_l^2} \sum_{i=1}^I |\mathcal{F} \{ \vec{w} \circ \bar{p}_k(t_i) \}|^2, \quad (9)$$

where  $\vec{w}$  is an analysis window—for example, a Hanning window—the same length as the summed pressure record,  $L = 2\Delta t$ ,  $F_s$  is the data sampling rate,  $\circ$  denotes the Hadamard (element-wise) product,  $I$  is the number of times  $\theta(t) = \theta_0$ , and  $\mathcal{F} \{ \bullet \}$  denotes the (one-sided Fast) Fourier transform.

This algorithm was applied to the recorded data from the rotor rig. For the given rotation speed and sampling rate, the number of samples per degree can be calculated to be 12. Therefore, to get meaningful frequency resolution, higher arc lengths must be analysed. In this case a  $5^\circ$  arc will be considered, corresponding to a rounded value of 61 samples per block. This value was then zero-padded, after applying a Hanning window, to a length of 256, providing a frequency resolution of 256 Hz.

The individual delayed pressure records were calculated by linearly interpolating between samples to the exact delay time, which is effective up to approximately  $F_s/4$ , beyond which the error becomes unacceptable.

The phase averaged beamforming results with  $\theta_0 = 0^\circ$  at selected frequencies are shown in Figure 7. These results are plotted with a reduced dynamic range due to the larger amount of background noise. The results clearly show dominant sound sources located near the tips of each rotor blade. As the frequency (and hence resolution) increases, it can be seen that much of the sound appears to come from the trailing-edge of the rotor blades near the tip. Other interesting features that warrant further investigation are the large sound source near

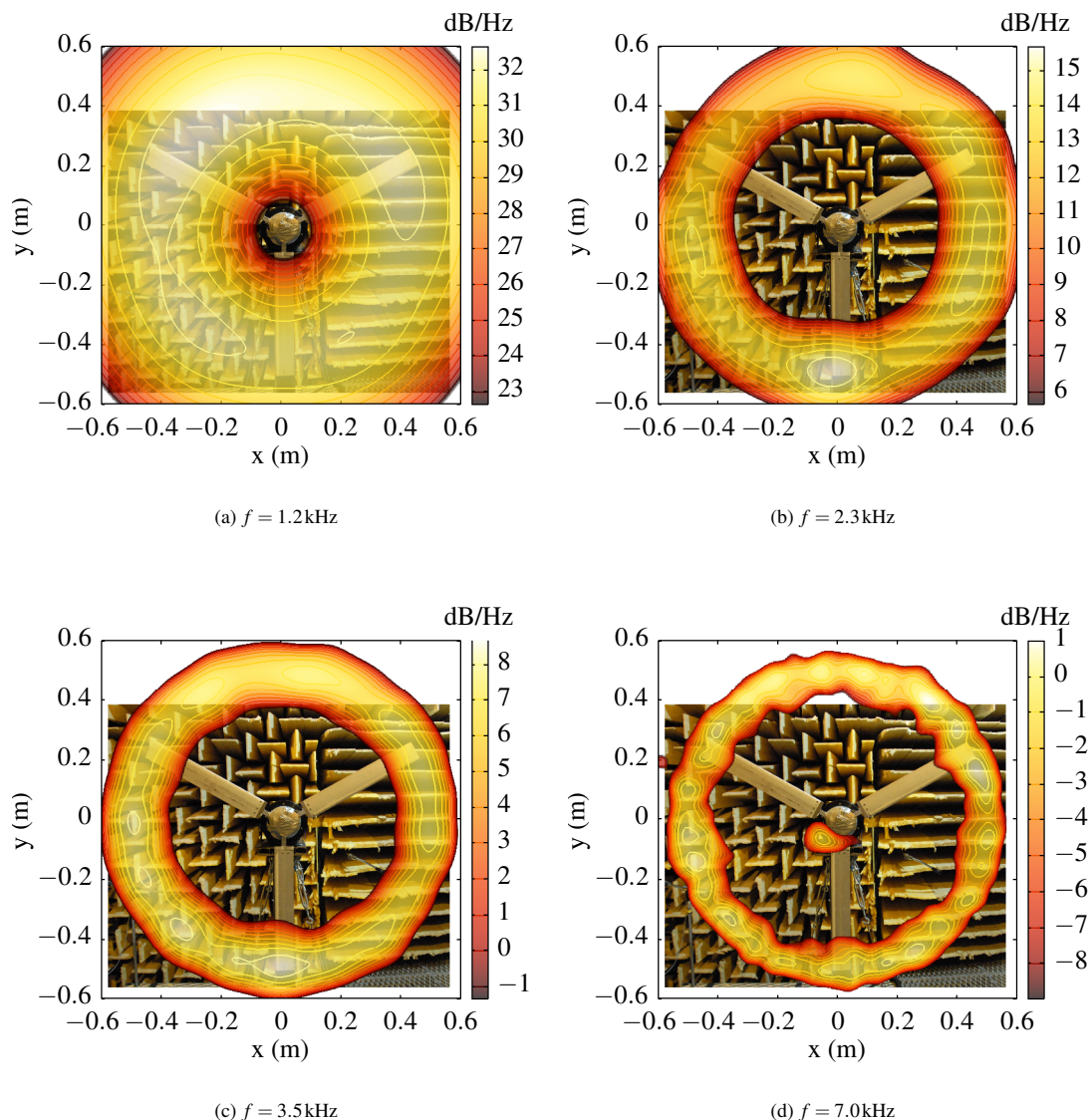


Figure 6 – Aggregate beamforming results for the rotor rig, running at 900 rpm in the Anechoic chamber at The University of Adelaide.

the post at 4.61 kHz, possibly due to a resonance in the rotor support structure, and the dual sources appearing at the tip at 12.8 kHz.

Frequencies lower than approximately 2 kHz performed poorly, most likely due to the small block sizes, leading to unreliable estimates of power at lower frequencies.

#### 4. CONCLUSIONS

The design and construction of the new School of Mechanical Engineering beamforming array has been presented. The microphone placement was selected using a bi-objective optimisation technique that allows the designer to trade off between array resolution and maximum side-lobe levels. In this case, it was found that a series of 7 concentric circles and 9 microphones per circle, gave the best performance.

As an example of the beamforming performance of this array, experimental results from a rotor rig experiment were presented, both in an aggregate and a phase averaged form. The aggregate results show that the largest sound contributions come from the tips of the rotors. Phase averaged results, although more noisy, were able to isolate contributions from both the leading-edge and the trailing-edge of the rotor tips at higher frequencies.

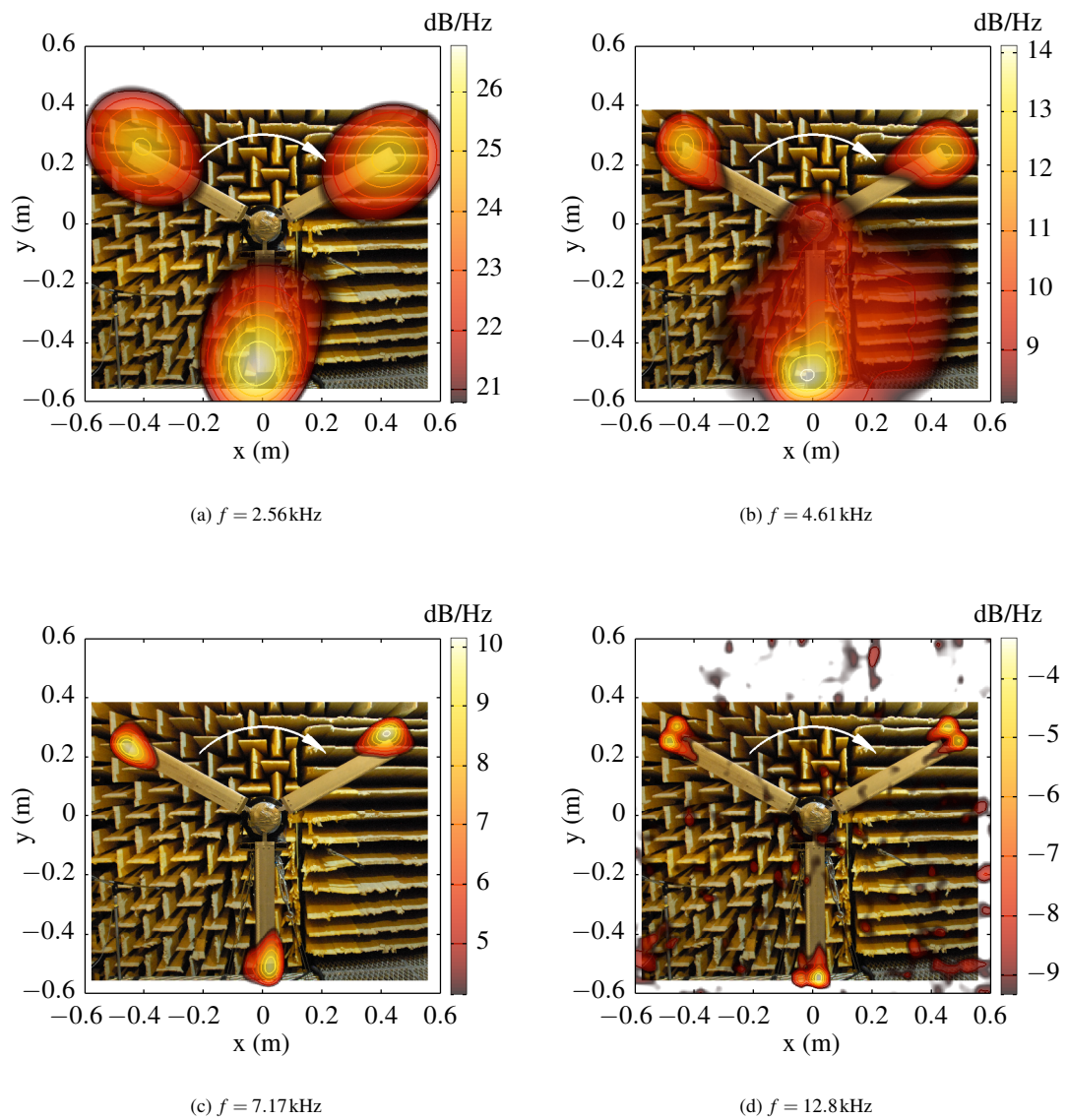


Figure 7 – Phase-averaged beamforming results of the rotor rig running at 900 rpm in the Anechoic chamber at The University of Adelaide for  $\theta_0 = 0^\circ$ . Note the reduced dynamic range of these plots (6 dB), used to help mask the increased noise due to lower signal levels.

## ACKNOWLEDGEMENTS

This work has been supported by the Australian Research Council, as part of ARC DP130103136.

## REFERENCES

1. Hald J, Christensen JJ. A novel beamformer array design for noise source location from intermediate measurement distances. *Journal of the Acoustical Society of America*. 2002;112(5):2448.
2. Christensen JJ, Hald J, inventors; Brüel; Kjær Sound; Vibration Measurement A/S, assignees. Beam forming array of transducers. US 7,098,865 B2; 2006.
3. Dougherty RP, inventor; The Boeing Company, assignee. Spiral-shaped array for broadband imaging. US 5,838,284; 1998.
4. Underbrink JR, inventor; The Boeing Company, assignee. Circularly symmetric, zero redundancy, planar array having broad frequency range applications. US 6,205,224 B1; 2001.
5. Underbrink JR. Aeroacoustic Phased Array Testing in Low Speed Wind Tunnels. In: Mueller TJ, editor. *Aeroacoustic Measurements*. Berlin: Springer; 2002. p. 98–217.
6. Prime Z, Doolan CJ. A comparison of popular beamforming arrays. In: *ACOUSTICS 2013*. 17–20 Nov., Victor Harbor, SA, AUS; 2013. .
7. Steinberg BD. *Principles of aperture and array system design: including random and adaptive arrays*. John Wiley & Sons; 1976.
8. Abramson MA, Audet C, Couture G, Dennis, Jr JE, Le Digabel S, Tribes C. The NOMAD project;. Software available at <http://www.gerad.ca/nomad>.
9. Le Digabel S. Algorithm 909: NOMAD: Nonlinear Optimization with the MADS algorithm. *ACM Transactions on Mathematical Software*. 2011;37(4):1–15.
10. Sarradj E. Three-Dimensional Acoustic Source Mapping with Different Beamforming Steering Vector Formulations. *Advances in Acoustics and Vibration*. 2012;2012.